Fuel 428 (2027) 140285

Contents lists available at ScienceDirect

Fuel

journal homepage: www.elsevier.com/locate/jfue

Full Length Article

Dynamic parameterization approach for MMC modeling of coal volatile combustion

Shiqi Meng [a], Tien Duc Luu [a], Ali Shamooni [b], Andreas Kronenburg [b], Oliver T. Stein [a,*]

[a] Engler-Bunte-Institute, Simulation of Reacting Thermo-Fluid Systems, Karlsruhe Institute of Technology, Karlsruhe, 76131, Germany
[b] Institute for Reactive Flows, University of Stuttgart, Stuttgart, 70569, Germany

HIGHLIGHTS

- Provide state-of-the-art CP-DNS validation datasets for volatile combustion from reacting solid fuel particles in HIT.
- Evaluate a coupled sparse-Lagrangian MMC-LES model for simulating reacting solid fuels.
- Analyse the sensitivity of particle mixing and two-phase coupling to various MMC parameters.
- Propose a novel methodology to determine MMC conditioning parameters dynamically.

ARTICLE INFO

Keywords:
Pulverized coal combustion
Sparse-lagrangian particle method
Multiple mapping conditioning
Dynamic parameterization

ABSTRACT

A sparse-Lagrangian particle implementation of the multiple mapping conditioning (MMC) model coupled to large eddy simulation (LES) for two-phase flows with reacting solid fuel particles is proposed. The MMC-LES model is developed and validated by means of carrier-phase direct numerical simulations (CP-DNS) of the devolatilization and volatile combustion from pulverized coal particles in statistically homogeneous isotropic turbulence (HIT). Two distinct Lagrangian particle clouds are introduced: The first cloud represents the inertial coal particles undergoing heat-up and pyrolysis, while the second cloud consists of stochastic MMC particles representing the reacting gas mixture of coal volatiles burning in air. To account for the heat and mass transfer between the two clouds, the one-to-one model for two-phase coupling in MMC is employed. To enhance model accuracy and practicality, a dynamic parameterization approach is proposed by deriving the governing MMC conditioning parameters, which are usually assumed to be constant, adaptively from the transient field of the volatile mixture fraction. Results show that conventional MMC predictions following best practice are in good agreement with the DNS for low fuel particle loadings, if suitable *a-priori* information (ideally from DNS) is available to calibrate the model. For high fuel particle loadings stronger deviations are observed. Moreover, we find that in conventional MMC the nominal conditioning parameters in physical and mixture fraction space r_m and f_m cannot be realized as physical and mixture fraction distances d_x and d_f for the most part of the transient ignition and volatile combustion process as expected. Differently, the new dynamic approach does not need *a-priori* calibration information from DNS, allows for a faithful match of the nominal and realized MMC conditioning parameters over time, and provides favorable predictions of the ignition and volatile combustion process. The sensitivity of the MMC results to the dynamic scaling factor α_f and constant C_ξ in the mixing time scale model is explored. A scaling factor $\alpha_f = 0.03$ is recommended, and while the standard value $C_\xi = 0.1$ already yields reasonable predictions, improved results can be obtained for slightly smaller C_ξ.

1. Introduction

Pulverized coal combustion (PCC) has been widely studied both experimentally and numerically due to its high relevance for energy conversion and because of its negative environmental impact associated with the emissions of CO_2, NO_x, SO_x and other pollutants [1–3]. PCC is a complex thermal conversion process involving two-phase heat transfer, devolatilization, homogeneous ignition, volatile combustion and heterogeneous surface reactions [4], bearing resemblance to solid fuel conversion processes like biomass combustion [5] and iron particle

* Corresponding author.
Email address: oliver.t.stein@kit.edu (O.T. Stein).

https://doi.org/10.1016/j.fuel.2026.140285
Received 20 March 2026; Received in revised form 19 May 2026; Accepted 5 June 2026
Available online 16 June 2026

oxidation [6]. The most accurate modeling approach for capturing solid fuel conversion processes is the boundary layer resolved simulation (BLRS) which fully resolves all physical and chemical processes in the gaseous near-field region of the reacting solid fuel particles [7,8]. However, BLRS is associated with very high computational costs and is therefore restricted to single particles and small particle groups [8,9].

For particle clouds, the necessity of resolving the particle boundary layer is relaxed and the carrier-phase direct numerical simulation (CP-DNS) approach is employed [4,10]. In CP-DNS, the particles are assumed to be Lagrangian point-particles where the heat and mass transfer across the boundary layer is modeled. However, at present, CP-DNS of reacting particle clouds is still limited to canonical configurations in the millimeter to centimeter size range and predictive simulations of particle combustion in more realistic solid fuel burners at the laboratory or even pilot scale require the large eddy simulation (LES) technique.

LES resolves the grid-scale variables while unresolved sub-grid terms require closure. One of the most important terms that require closure is the highly non-linear chemical source term [11]. The Filtered Density Function (FDF) method for LES [12,13] provides a promising approach for combustion LES, since the chemical source terms appear in closed form. Due to its high dimensionality, it is impractical to solve the FDF transport equation directly in the Eulerian framework, such that stochastic particle methods, which approximate FDF solutions, are more commonly employed [14,15]. As the computational cost of stochastic FDF-LES methods becomes very high for large numbers of stochastic particles, the Multiple Mapping Conditioning (MMC) model [16] can be applied to substantially reduce the required particle number. The central concept of MMC-LES is the *conditioning* of stochastic particle pair mixing on suitable reference variables such that scalar diffusion at the sub-grid scale can efficiently and accurately be modeled with a small number of stochastic particles (approximately one stochastic particle per LES cell). The mixture fraction has been established as a reliable conditioning variable for non-premixed gaseous [17,18] and non-premixed multiphase combustion [19–21]. However, for multiphase combustion, additional modeling challenges arise: In multiphase MMC-LES, the reacting gas phase is represented by one set of stochastic particles, while another particle set is required to represent the fuel particles. Since the two different phases need to exchange heat and mass, a two-phase coupling method for MMC is required. For droplet combustion, Khan et al. [19] suggested a one-to-one coupling method, in which for each fuel droplet a corresponding stochastic particle is selected based on their proximity in physical and reference space (mixture fraction). The same coupling method has been applied by Kirchmann et al. [20] and was further explored by Sontheimer et al. [21,22], who assessed the limitations of the one-to-one coupling method and compared it with alternative coupling approaches using detailed CP-DNS data for evaluation.

To the authors' knowledge, the only study that has previously attempted to model coal particle combustion by means of MMC-LES is the work of Zhao et al. [23]. In that work, the devolatilization and volatile combustion process of pulverized coal particles in a piloted laboratory jet flame was simulated and validated against experimental data. Although the turbulent velocity field was predicted accurately, the reacting scalar fields were still associated with considerable experimental and numerical uncertainties. Moreover, in [23], the governing MMC conditioning parameters were estimated empirically and kept constant during the simulation, as is conventional in MMC-LES. In light of this, the present paper addresses the following major objectives:

- **Provide reliable validation data:** We provide state-of-the-art validation data for MMC-LES modeling by conducting CP-DNS calculations of coal particle cloud devolatilization and volatile combustion. To focus on the modeling of turbulence-particle-chemistry interactions under well-defined conditions, we restrict ourselves to coal particles burning in statistically homogeneous isotropic turbulence (HIT).
- **Estimate the MMC conditioning parameters:** We estimate the MMC conditioning parameters for mixing and two-phase coupling by (i) using standard assumptions and constant parameters and (ii) proposing a method to dynamically determine the conditioning parameters.

We note that the present study bears some resemblance to the previous work by Sharma et al. [24] who developed a dynamic model for the mixing time scale in single-phase MMC. Instead, here we adhere to a standard model for the mixing time scale, but investigate a dynamic model for the MMC conditioning parameters, i.e., mixing and two-phase coupling.

2. Modeling

2.1. Carrier-phase DNS

In CP-DNS, the gas phase is described by the instantaneous governing equations in their variable-density formulation. The governing equations of mass, momentum, sensible enthalpy and chemical species are solved, containing additional source terms due to mass, momentum and heat exchange with the Lagrangian solid phase [4,23]. For the present HIT setup, the momentum equation contains a forcing term following Bassenne et al. [25] to ensure that turbulence does not decay prior to interacting with the particles and the subsequent volatile combustion process. For MMC, an additional transport equation for the volatile mixture fraction f is solved

$$\frac{\partial \rho f}{\partial t} + \frac{\partial}{\partial x_i}\left(\rho u_i f\right) = \frac{\partial}{\partial x_i}\left(\frac{\mu}{\mathrm{Sc}}\frac{\partial f}{\partial x_i}\right) + \dot{S}_m \tag{1}$$

where t is time, x and subscripts $< i, j >$ indicate the spatial coordinate directions, and ρ, u, μ and $\mathrm{Sc}\,(=0.7)$ are the density, velocity, dynamic viscosity, and Schmidt number of the gas mixture. The source term $\dot{S}_m$ accounts for the release of volatiles from the coal particles to the gas phase and equally appears in the continuity equation. The modeling of the Lagrangian coal particles follows our previous work [4,10,26]. The coal particles exchange momentum with the gas phase due to drag and two-phase heat exchange is realized via Nusselt number correlations (Ranz-Marshall). A unity Lewis number is assumed for the gas phase. Devolatilization is described by a two-step competing rate model [27], whereas char conversion and radiation are neglected in the present work. For further details on the treatment of the Lagrangian fuel particles we refer the reader to Rieth et al. [4,10].

We note that the present CP-DNS represents the early stages of the coal combustion process, during which particle heat-up, ignition and volatile combustion are dominant. Char conversion becomes significant only at later stages of combustion, which require substantially longer particle residence times and are therefore extremely difficult to tackle with DNS. Moreover, this work primarily aims to evaluate the initial two-phase MMC formulation for devolatilization and volatile combustion without introducing the additional complexity of char conversion. Including char conversion would require additional closures for particle-surface reactions, particle heat and mass transfer, the possible overlap between devolatilization and char conversion [28], and their coupling with the stochastic MMC particles. Therefore, the present two-phase MMC model is restricted to devolatilization, gas-phase mixing, and chemical reactions associated with volatile combustion [23].

2.2. Two-phase MMC modeling

The FDF transport equation is solved by a set of equivalent stochastic differential equations that govern the motion, chemical state and mass of the stochastic particle ensemble representing the turbulent gas phase [19,21,23]

$$\mathrm{d}x_i^{sp} = \left[\widetilde{u}_i + \frac{1}{\overline{\rho}}\frac{\partial \overline{\rho} D_{\mathrm{eff}}}{\partial x_i}\right]^{sp}\mathrm{d}t + \left[\sqrt{2D_{\mathrm{eff}}}\right]^{sp}\mathrm{d}\omega_i, \tag{2}$$

$$\mathrm{d}\phi_k^{sp} = \left[W_k^{sp} + \langle M_k|\widetilde{\boldsymbol{\psi}}\rangle^{sp} + (\phi_k^{*,fp} - \phi_k^{sp})\langle \Pi|\widetilde{\boldsymbol{\psi}}\rangle^{sp}\right]\mathrm{d}t, \tag{3}$$

$$\mathrm{d}m^{sp} = m^{sp}\langle \Pi | \widetilde{\boldsymbol{\psi}} \rangle^{sp} \mathrm{d}t, \tag{4}$$

where Eq. (2) gives the position of the stochastic particle (sp), $\tilde{\cdot}$ indicates Favre-filtered quantities, $\mathcal{D}_{\mathrm{eff}}$ is the effective diffusivity and $\mathrm{d}\omega_i$ is the increment of a stochastic Wiener process. Eqn. (3) expresses the stochastic particle state, where $\boldsymbol{\phi} = (\boldsymbol{Y}, h)$ is the gas composition vector with composition index k, species mass fraction vector $\boldsymbol{Y}$ and sensible enthalpy h. The chemical source term W_k^{sp} for species k is evaluated directly from the composition vector of the stochastic particle and is therefore closed. $\langle \cdot | \widetilde{\boldsymbol{\psi}} \rangle$ is a quantity that is filtered conditionally on the vector of reference variables $\widetilde{\boldsymbol{\psi}}$. M_k is the mixing term, Π refers to the devolatilization rate, and the term $\phi_k^{*,fp}$ denotes scalar quantities at the fuel particle (fp) which attain different mathematical expressions depending on the individual state variable ($\boldsymbol{Y}$ or h) [23]. Finally, Eq. (4) calculates the stochastic particle mass which can change because of devolatilization processes.

Eqs. (2)–(4) are directly valid for a posteriori applications of MMC-LES, similar to the work by Zhao et al. [23]. Here, we evaluate the MMC model a priori based on post-filtering the instantaneous CP-DNS data. Post-filtering is implemented by generating an auxiliary LES grid coarser than the CP-DNS mesh and explicitly Favre-filtering the Eulerian CP-DNS data on the secondary LES mesh [18]. In this way, LES-like quantities are obtained and interpolated to the stochastic particle location as indicated by the operator $\widetilde{(\cdot)}^{eu}(\mathbf{x}^{sp})$. Applying this procedure to the reference mixture fraction and effective diffusivity yields

$$f^{sp} = \widetilde{f}^{eu}(\mathbf{x}^{sp}), \tag{5}$$

$$D_{\mathrm{eff}}^{sp} = \widetilde{D_{\mathrm{eff}}}^{eu}(\mathbf{x}^{sp}) = \widetilde{\mathcal{D}}^{eu}(\mathbf{x}^{sp}) + \widetilde{\mathcal{D}}_t^{eu}(\mathbf{x}^{sp}), \tag{6}$$

with the laminar diffusivity $\widetilde{\mathcal{D}}^{eu}$ and the turbulent diffusivity $\widetilde{\mathcal{D}}_t^{eu}$ further explained below. The mixing operator M_k in Eq. (3) is closed by mixing a pair of stochastic particles p and q similarly to Curl's model [29]

$$\phi_k^p(t+\Delta t) = \phi_k^p(t) + \gamma\left(\bar{\phi}_k^{p,q}(t) - \phi_k^p(t)\right), \tag{7}$$

$$\phi_k^q(t+\Delta t) = \phi_k^q(t) + \gamma\left(\bar{\phi}_k^{p,q}(t) - \phi_k^q(t)\right), \tag{8}$$

where Δt is the computational time step, $\bar{\phi}_k^{p,q}$ is the average composition of stochastic particles p and q, and the mixing extent γ is calculated as

$$\gamma = 1 - \exp\left(-\Delta t/\tau_L\right) \tag{9}$$

with τ_L being the Lagrangian time scale for stochastic particle pair mixing. We model τ_L using the anisotropic *a-ISO* mixing time scale model proposed by Vo et al. [18] as

$$\tau_L = \frac{C_\xi d_x^2}{2\left[\widetilde{\mathcal{D}}^{eu}(\mathbf{x}^{sp}) + \mathcal{D}_{t,L}\right]}, \tag{10}$$

where C_ξ is a model parameter (usually set to 0.1), d_x is the physical space distance between stochastic particles in a pair (see Eq. (12) below) and $\mathcal{D}_{t,L}$ is the turbulent sub-grid scale diffusivity that acts at the relevant Lagrangian length scales defined as $\mathcal{D}_{t,L} = \frac{d_x}{\Delta_E}\widetilde{\mathcal{D}}_t^{eu}(\mathbf{x}^{sp})$. Note that parameter C_ξ in Eq. (10) is usually denoted as C_f in the common MMC literature [18,24], but renamed here to avoid ambiguity with case C-f that will be introduced in Section 3.2.

In line with the MMC-LES modeling approach, the turbulent diffusivity $\mathcal{D}_t^{eu}$ for MMC is obtained by using an LES turbulence model, and in the present work we use the Smagorinsky model. However, following the DNS-based assessment strategy used in previous MMC-LES studies to isolate MMC modeling errors from flow field errors associated with LES models [18], $\mathcal{D}_t$ in Eq. (6) is set to zero in the present a priori study, and the filtered velocity and density in Eq. (2) are replaced by their instantaneous counterparts available from CP-DNS. This procedure avoids uncertainties from the turbulence model affecting the stochastic particle motion and allows us to assess the MMC mixing and two-phase coupling models under prescribed DNS-based flow conditions. It should therefore be noted that the present a priori evaluation does not include errors associated with the LES turbulence closure, resolved-flow evolution, or unresolved velocity fluctuations. Consequently, the reported agreement should not be interpreted as a full measure of the predictive accuracy of a coupled a posteriori MMC-LES model, but rather as an idealized case estimate.

The MMC mixing operation $\langle M_k | \widetilde{\boldsymbol{\psi}} \rangle^{sp}$ is localized by selecting stochastic particle pairs that are close in both physical and reference mixture fraction space, i.e., $\widetilde{\boldsymbol{\psi}} = \psi(x_i, \tilde{f})$. This is achieved by minimizing the effective squared distance between stochastic particle pairs according to

$$\hat{d}_{p,q}^2 = \sum_{i=1}^{3}\left(\sqrt{3}\frac{d_{x_i}^{p,q}}{r_m}\right)^2 + \left(\frac{d_f^{p,q}}{f_m}\right)^2, \tag{11}$$

where $d_{x_i}^{p,q} = |x_i^p - x_i^q|$ and $d_f^{p,q} = |\tilde{f}(\mathbf{x}^p) - \tilde{f}(\mathbf{x}^q)|$ are the distances in physical and mixture fraction space between particles p and q, while r_m and f_m are their nominal counterparts that are used as inputs to the simulation to control mixing. Analogously, the pairs of fuel and stochastic particles for one-to-one coupling in two-phase flows [19,21,22] are selected according to

$$\hat{d}_{fp,sp}^2 = \sum_{i=1}^{3}\left(\sqrt{3}\frac{d_{x_i}^{fp,sp}}{r_m^*}\right)^2 + \left(\frac{d_f^{fp,sp}}{f_m^*}\right)^2, \tag{12}$$

where $d_{x_i}^{fp,sp} = |x_i^{fp} - x_i^{sp}|$ and $d_f^{fp,sp} = |\tilde{f}(\mathbf{x}^{fp}) - \tilde{f}(\mathbf{x}^{sp})|$ are the distances in physical and mixture fraction space between fuel particle fp and stochastic particle sp, and f_m^* and r_m^* are their nominal values used to control two-phase coupling. While the minimization in Eq. (11) is implemented via the k-d tree algorithm, Eq. (12) uses a direct minimization technique [22] since the number of stochastic and fuel particles is generally not the same.

Following the isoscalar sliver concept of Cleary et al. [17] the nominal mixing control parameters r_m and f_m in Eq. (11) are related to each other according to

$$r_m = C_m\left(\frac{d\tilde{f}}{dn}\frac{\Delta_L^3}{r_c^{2-D_f}}\frac{1}{f_m}\right)^{1/D_f}, \tag{13}$$

where $C_m = 0.5$, Δ_L is the average distance of the stochastic particles (estimated as the inverse of the cube root of the particle number density), r_c is the cut-off length taken as the size of the LES mesh for post-filtering Δx_{LES} and $D_f = 2.36$ is the fractal dimension of turbulence [30]. The LES mixture fraction gradient $d\tilde{f}/dn$ needs to be estimated from a characteristic location in the flow and was extracted from the shear layer of a jet flame in [17]. In the present work, we take $d\tilde{f}/dn$ as the maximum value of the post-filtered mixture fraction field.

2.3. Conventional and dynamic parameter models

The nominal mixture fraction distance f_m is one of the major control parameters for MMC. While $f_m = 0.03$ has been established as a standard parameter for single-phase flows where the maximum mixture fraction is 1.0 [18], Sontheimer et al. noted that the peak mixture fraction in two-phase flows is considerably smaller and suggested a scaling method for f_m [21]. In this method, a DNS is performed in advance, followed by an LES-like filtering procedure to determine the domain-wide maximum filtered mixture fraction $\tilde{f}_{max}$ for subsequent use in MMC. A suitable value of f_m is then estimated by multiplying the standard value $f_m = 0.03$ by $\tilde{f}_{max}$. In the present work, we generate a first set of *conventional MMC* results by using constant MMC conditioning parameters following best practices in line with [21].

However, in two-phase flows, especially in transient particle devolatilization and burning, the maximum mixture fraction can change

significantly over time as devolatilization progresses, limiting the universality of the conventional method. The difficulty is that MMC conditioning relies on a measure of locality in the conditional scalar space, whereas the relevant scalar range continuously evolves in transient two-phase reacting flow systems. Therefore, a fixed value of f_m may correspond to different relative conditioning distances across the transient process, leading to inconsistent particle pair selection and case-dependent parameter specification. Therefore, we propose a dynamic procedure for MMC conditioning as

$$f_m(t) = \alpha_f \left[\tilde{f}_{\max}(t) - \tilde{f}_{\min}(t)\right], \tag{14}$$

at every time step, with $\tilde{f}_{\min}(t)$ and $\tilde{f}_{\max}(t)$ being the minimum and maximum instantaneous values of the filtered mixture fraction, and α_f a scaling factor. In the current study, the proposed dynamic model is examined using the HIT configurations presented in Section 3.1 and $f_{\max}$ and $f_{\min}$ are determined from the instantaneous extrema of the filtered mixture fraction field over the entire computational domain. This global definition is consistent with the statistically homogeneous nature of HIT, where no mean shear, recirculation, wall-bounded, or clearly separated local flow region exists. However, for spatially inhomogeneous flames, domain-wide extrema may not fully represent the local mixing state. A physically localized evaluation of $f_{\max}$ and $f_{\min}$ may therefore be more appropriate, possibly guided by further locality considerations such as the inertial-subrange constraint on physical space distance discussed in our previous work [23] and others. Although this was not adopted in that study nor in the present HIT configuration, it provides a useful direction for future extension.

Moreover, this dynamic procedure for MMC mixing is also extended to MMC two-phase coupling in a simple manner as follows: Sontheimer performed a detailed analysis of the high-dimensional space comprising the nominal physical and mixture fraction distances, as well as further conditioning parameters [31]. This analysis led to a recommended ratio of the nominal MMC mixing to two-phase coupling parameters of

$$r_m/r_m^* = f_m/f_m^* = 1.66. \tag{15}$$

A sensitivity analysis was performed by varying the value of 1.66 by $\pm 50\%$. As shown in Appendix D, the predicted results are only weakly affected by this variation for the present case, hence the original value of 1.66 is retained.

3. Computational configuration and model parameters

3.1. CP-DNS configurations

We perform CP-DNS and simultaneous *a priori* MMC-LES modeling of pulverized coal particles. The coal particles undergo heat-up, devolatilization, homogeneous ignition and volatile combustion in statistically homogeneous isotropic turbulence. The initial turbulence field, before adding the coal particles, is forced to attain a constant Taylor Reynolds number $\mathrm{Re}_\lambda = 30$, with an integral length scale $l_{\mathrm{int}} = 1.90$ mm. Moreover, turbulent forcing is retained during the subsequent calculation of the reacting two-phase flow to ensure that turbulence does not decay while interacting with the coal particles. The edge length $L_x = 12.0$ mm of the cubic computational domain is chosen to be approximately 6 times the integral length scale. A 160^3 mesh is used for the DNS, ensuring that the cell size $\Delta x_{DNS} = 75.0$ μm is smaller than the Kolmogorov length scale $\eta \approx 90.2$ μm.

Pulverized coal is represented by an ensemble of spherical particles distributed randomly and homogeneously across the domain at the beginning of the reacting flow simulation. To ensure the validity of the point-particle assumption for CP-DNS [5] the fuel particle size is set to $d_{fp} = 15$ μm ensuring a ratio $\Delta x_{DNS}/d_{fp} = 5.0$. The detailed description of the coal properties follows Rieth et al. [4]. The density of the coal particles is set to 1000 kg/m^3. The initial mass fractions of volatiles, fixed char and ash inside the coal particles are 0.592, 0.325 and 0.083, respectively. To maintain computational tractability of the gas-phase kinetics, the tar species are collectively represented by C_2H_2 [23] and the DRM-22 skeletal mechanism, involving 104 elementary reactions and 22 chemical species [32] is used to model coal volatile combustion. The DRM-22/C_2H_2 kinetic description was compared against the more detailed CRECK-52 scheme, in which C_6H_6 is used as the tar surrogate [4,7]. The comparison was performed using 0-D ignition delay simulations under the relevant thermochemical conditions of the 3D cases. At the temperatures corresponding to the (mean) ignition times extracted from the 3D cases, the two mechanisms yield nearly identical ignition delay times (plots omitted for brevity), supporting the use of DRM-22/C_2H_2 in the present simulations. The detailed description of the volatiles follows Zhao et al. [23], and the assumed coal and volatile compositions corresponding to Newlands bituminous coal are summarized in Table 1. The initial composition of the surrounding gas is $Y_{N_2} = 0.7121$, $Y_{O_2} = 0.1407$, $Y_{CO_2} = 0.1153$ and $Y_{H_2O} = 0.0319$. This is in analogy to Rieth et al. [4], where fresh coal particles were entrained into a partially reacted mixture of coal volatiles with air. In this way, the heat from the partial volatile/air oxidation and some remaining oxygen is provided to trigger the heat-up, devolatilization and volatile combustion of the freshly inserted coal particles during the simulation. This initialization of the simulations mimics the situation occurring in the shear layers of turbulent coal combustors, where fresh particles are subjected to recirculated, (partially-)reacted combustion products [4,10]. The initial temperatures of the fuel particles and surrounding gas phase are set to $T_{fp} = 693$ K and $T_g = 1393$ K, respectively. The reference case for the present simulations features a global equivalence ratio of $\phi = 1.0$ which corresponds to a fuel particle number $N_{fp} = 23{,}265$ and is referred to as case ϕ-M in Table 2. To investigate the effect of coal particle loading on the MMC-LES model, two additional cases ϕ-L and ϕ-H in Table 2 with global equivalence ratios of 0.66 and 1.97 have been explored. We also note that, while we have attempted to set material properties representative of realistic coal particle ignition and burning, the exact details of the coal sub-model (while maintained in a reasonable range) are only of secondary importance for the present model evaluation.

Table 1
Mass fractions of coal particle components [4,23].

Phase	Mass fraction	Species	Mass fraction
Gas	0.592	CH_4	0.082
		C_2H_2	0.595
		C_2H_4	0.088
		CO	0.052
		H_2	0.009
		N_2	0.034
		CO_2	0.041
		H_2O	0.099
Solid	0.408	Ash	0.2034
		Fixed Carbon	0.7966

Table 2
CP-DNS configurations.

Case	ϕ	N_{fp}	m_{fp} (kg)
ϕ-L	0.66	15,286	$2.70\cdot10^{-8}$
ϕ-M	1.00	23,265	$4.11\cdot10^{-8}$
ϕ-H	1.97	45,857	$8.10\cdot10^{-8}$

3.2. MMC-LES

The CP-DNS data is post-filtered on an LES mesh with 20^3 cells, such that $\Delta x_{LES} = 8\Delta x_{DNS} = 0.6$ mm. As a base case, 8000 stochastic particles are used, corresponding to a typical sparse MMC-LES resolution of 1L/1E, i.e., one stochastic particle per LES cell. To also assess the model accuracy for even sparser MMC conditions, two additional configurations with one stochastic particle per two and four LES cells, i.e., 1L/2E and 1L/4E are also explored. To evaluate the accuracy of the MMC

Table 3
Constant parameter sets for *conventional MMC*.

Cases	Sets	f_m	r_m (mm)	f_m^*	r_m^* (mm)
1L/1E					
ϕ-L	C-f	0.0007	20.78	0.0004	12.52
	C-m	0.0021	1.06	0.0013	0.64
	C-r	1.0	0.006	0.60	0.0036
ϕ-M	C-f	0.0009	20.78	0.0005	12.52
	C-m	0.0031	0.98	0.0019	0.59
	C-r	1.0	0.006	0.60	0.0036
ϕ-H	C-f	0.0014	20.78	0.0008	12.52
	C-m	0.0041	0.89	0.0025	0.54
	C-r	1.0	0.006	0.60	0.0036
1L/2E					
ϕ-L	C-f	0.0007	20.78	0.0004	12.52
	C-m	0.0021	1.44	0.0013	0.87
	C-r	1.0	0.0076	0.60	0.0046
ϕ-M	C-f	0.0009	20.78	0.0005	12.52
	C-m	0.0031	1.42	0.0019	0.85
	C-r	1.0	0.0076	0.60	0.0046
ϕ-H	C-f	0.0014	20.78	0.0008	12.52
	C-m	0.0041	1.20	0.0025	0.72
	C-r	1.0	0.0076	0.60	0.0046
1L/4E					
ϕ-L	C-f	0.0007	20.78	0.0004	12.52
	C-m	0.0021	1.91	0.0013	1.15
	C-r	1.0	0.0095	0.60	0.0057
ϕ-M	C-f	0.0009	20.78	0.0005	12.52
	C-m	0.0031	1.75	0.0019	1.05
	C-r	1.0	0.0095	0.60	0.0057
ϕ-H	C-f	0.0014	20.78	0.0008	12.52
	C-m	0.0041	1.60	0.0025	0.96
	C-r	1.0	0.0095	0.60	0.0057

model, the CP-DNS cases ϕ-L, ϕ-M and ϕ-H from Table 2 are modeled using various sets of parameters for MMC mixing (f_m, r_m) and MMC two-phase coupling (f_m^*, r_m^*). Both *constant parameters* and *dynamic scaling* are employed, with the constant values given in Table 3. Parameter sets named C-f refer to strict conditioning on the reference mixture fraction and use values $f_m = 0.01 \cdot \tilde{f}_{max}$ (i.e., 1% of the peak filtered mixture fraction), while r_m is set to the diagonal of the cubic domain ($r_m = 20.78$ mm), which is the maximum possible physical coupling distance of the HIT setup. Conversely, parameter sets denoted C-r refer to strict conditioning in physical space, where $r_m = 0.01 \cdot \Delta_L$ (i.e., 1% of the average stochastic particle distance) and $f_m = 1.0$ to allow for large mixture fraction distances. Parameter sets named C-m follow best practices in conventional two-phase MMC and scale f_m based on $\tilde{f}_{max}$ such that $f_m = 0.03 \cdot \tilde{f}_{max}$ and calculate r_m using Eq. (13). We note that cases C-f and C-r are both over-constraining the particle pairing process, while C-m is considered to be a reasonable parameter set for conventional MMC. For all sets, to ensure consistent MMC mixing and two-phase coupling, the ratio 1.66 between the mixing and two-phase coupling parameters extracted from the DNS database of [31] is used, i.e., Eq. (15) applies.

The *dynamic scaling* approach follows Eq. (14), where the minimum and maximum filtered mixture fractions are extracted from the simulation at every time step, while the scaling factor α_f requires calibration. In the present study, we test α_f values of 0.01, 0.03, and 0.09, similar to the suggested values of f_m in conventional MMC [17,22]. After determining f_m from Eq. (14), the corresponding r_m is computed using Eq. (13), while f_m^* and r_m^* follow from Eq. (15). As a result, all four control parameters of two-phase MMC are adjusted dynamically at every time step of the simulation.

Finally, we explore the universality of the parameter C_ξ in the mixing time scale expression of the *a-ISO* model, Eq. (10), for the present case. While its standard value is 0.1, Sharma et al. [24] pointed out that, at almost all spatial locations of their turbulent gas jet flame calculations, $C_\xi < 0.1$ was more appropriate. For the present case of transient coal particle ignition and volatile burning we re-evaluate the effect of C_ξ across the range [0.01, 0.5].

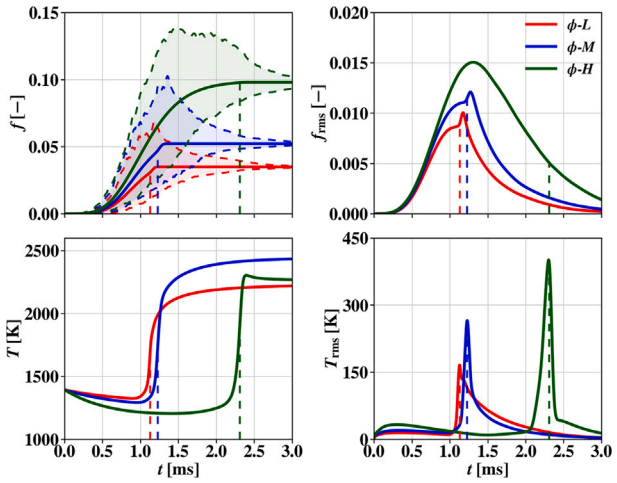

Fig. 1. Temporal evolution of the mixture fraction (top row) and gas temperature (bottom row) for various fuel particle loadings from CP-DNS. Left column: Means (continuous lines) obtained by averaging over the 3D computational domain at every time step. Right column: RMS values quantifying deviations from the mean. The dotted curves in the top left panel indicate the minimum and maximum LES-filtered mixture fraction $\tilde{f}_{\max}$ inside the 3D domain for MMC-LES modeling. The dashed vertical lines in all panels indicate the ignition (delay) times extracted as the times when the peak gradient of the mean gas temperature is attained (see bottom left panel). (For interpretation of the references to color in this figure legend, the reader is referred to the web version of this article.)

3.3. Solver settings

Simulations are run up to a physical time of 3.0 ms using a constant time step $\Delta t = 5.0 \times 10^{-7}$s which corresponds to a maximum CFL number ≤ 0.3. A pressure-based variable-density OpenFOAM flow solver coupled with in-house MMC libraries is used [33].

4. Results

Section 4.1 will present the results from the CP-DNS cases and discuss their major characteristics. Subsequently, Section 4.2 will show predictions obtained by conventional MMC-LES and evaluate them by comparison to the DNS data. Finally, Section 4.3 will present MMC results from the dynamic model and provide an estimate for suitable values of the dynamic scaling parameter α_f, followed by the evaluation of the *a-ISO* mixing time scale model parameter C_ξ.

4.1. Carrier-phase DNS results

Prior to assessing the MMC-LES model, we first explore the effect of fuel particle loading (global equivalence ratio) on the heat-up, homogeneous ignition and volatile combustion characteristics based on the CP-DNS database, i.e., discuss the results from cases ϕ-L, ϕ-M and ϕ-H in Table 2. Fig. 1 presents the temporal evolution of volatile mixture fraction and gas temperature in terms of mean and root mean square (RMS) values obtained by averaging over the 3D computational domain at every CP-DNS time step. Fig. 1 (top left) shows the mean CP-DNS mixture fraction (continuous lines) accompanied by the corresponding minimum and maximum values (dashed curves) after LES-filtering as a function of time. The LES-filtered values will be considered later, for MMC modeling. Initially all particles still contain their full volatile content such that the volatile mixture fraction starts at zero. Subsequently, particles are heated up by the surrounding gas which -in turn- initially loses heat to the solid phase, see mean gas temperatures in Fig. 1 (bottom

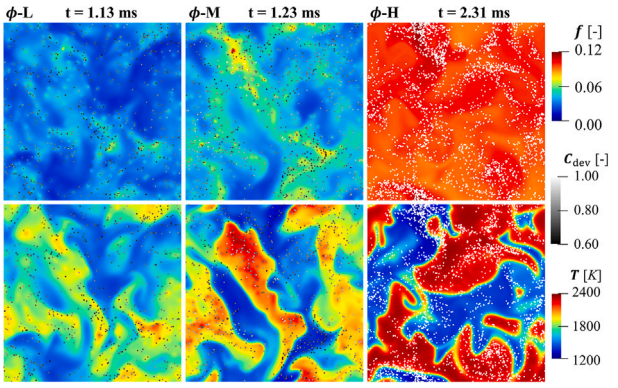

Fig. 2. Contour plots (y-z slice for $x = L_x/2$) of mixture fraction (top row) and gas temperature (bottom row) for the different fuel particle loadings at their respective mean ignition times, see dashed vertical lines in Fig. 1 (bottom left). Only particles located within $0.50L_x \leq x \leq 0.55L_x$ are shown. The particle devolatilization progress C_{dev} [4] is shown in grayscale, where only the range $0.6 \leq C_{dev} \leq 1.0$ is shown for clarity and $C_{dev} = 1.0$ indicates fully devolatilized particles. (For interpretation of the references to color in this figure legend, the reader is referred to the web version of this article.)

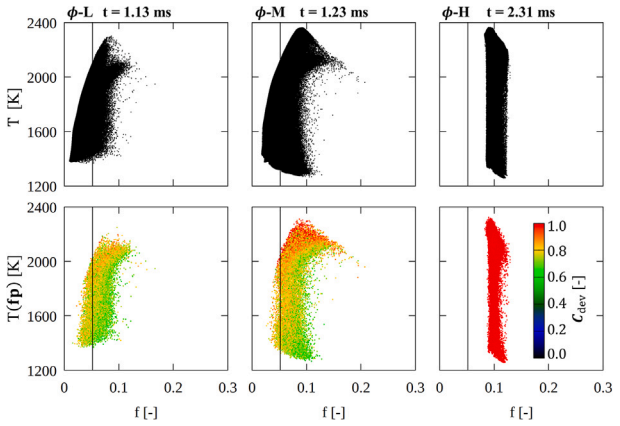

Fig. 3. Scatter plots of gas temperature vs. mixture fraction from the CP-DNS at the times of ignition for cases ϕ-L, ϕ-M and ϕ-H. Scatter data from the entire computational domain (top). Scatter data solely extracted from the Eulerian cells in which coal particles reside colored by their devolatilization progress (bottom). The black vertical line indicates the stoichiometric mixture fraction $f_{st} = 0.052$. (For interpretation of the references to color in this figure legend, the reader is referred to the web version of this article.)

left). Particle heat-up induces devolatilization such that the peak mixture fraction in Fig. 1 (top left) starts to deviate from zero at around 0.3 ms for all cases, followed by a rapid increase of the mean mixture fraction and subsequent saturation to a final mean value of ≈0.035, ≈0.052 and ≈0.1 for cases ϕ-L (red), ϕ-M (blue) and ϕ-H (green), respectively, with the saturation time shifting progressively to later times in the same order. This saturation effect is expected, since for all cases, the coal particles fully release their volatiles during the simulation, such that volatile depletion leads to flat profiles of the mean volatile mixture fraction at late times. The range of filtered mixture fractions (distance between the upper and lower dashed lines, used in *dynamic MMC*, Eq. (14)) also increases from initially zero to peaks in the time range [1.2 ms, 1.5 ms], before narrowing down to nearly zero deviation from the mean value at late times.

The mean gas temperature profiles for all three cases are shown in Fig. 1 (bottom left), where a higher coal mass loading leads to initially stronger heat losses of the gas phase to the particles, followed by ignition and volatile combustion, with ϕ-M reaching the highest gas temperatures of all three cases at late times because fuel and air are available in stoichiometric proportions for this case. Moreover, the final mean temperature of the rich case ϕ-H is higher than that of the lean case ϕ-L. This trend is confirmed by 0D simulations of lean and rich volatile/air mixtures (not shown for brevity) and is related to the higher heat capacity of the volatiles compared to the background gas.

For later analysis, we extract ignition (delay) times from the gas temperatures defined as the time when the mean gas temperature attains its maximum gradient. The ignition times (t_{ign}) thus obtained are 1.13 ms for case ϕ-L, 1.23 ms for case ϕ-M and 2.31 ms for case ϕ-H and are shown as dashed vertical lines in Fig. 1. The RMS mixture fraction profiles in Fig. 1 (top right) indicate a monotonous trend of increasing RMS levels and consistently later RMS peaks with higher equivalence ratios. Similarly, the RMS of the gas temperature shown in Fig. 1 (bottom right) exhibits both delayed and higher RMS peaks with increasing ϕ, with the peaks of T_{rms} matching the previously extracted ignition times. This indicates that at the (averaged) ignition time there is significant spatial variation inside the 3D domain, where regions with few coal particles are not surrounded by burning volatiles yet, whereas the gas in regions where many particles have previously released their volatiles is burning. At late times both the RMS of mixture fraction and temperature tend towards zero, as turbulent mixing acts to reduce the spatial gradients.

For further illustration, Fig. 2 shows instantaneous contour plots of the mixture fraction (top row) and gas temperature (bottom row) at the previously extracted mean ignition times of the three CP-DNS cases. In line with Fig. 1, it can be observed that the mixture fraction levels increase with equivalence ratio, with the richest case ϕ-H exhibiting the smallest spatial variations (smallest f_{rms}) during ignition. This is because the delayed ignition of case ϕ-H compared to cases ϕ-L and ϕ-M occurs at a time when particles have already fully released (on average) their volatile content, while the ignition of cases ϕ-L and ϕ-M already happens during the final stages of (mean) devolatilization, see f in Fig. 1. This is attributed to the strongest initial mean heat loss of the gas phase to the coal particles that occurs for case ϕ-H, i.e., the green line T in Fig. 1. The spatial variations of gas temperature in Fig. 2 (bottom) are comparable for cases ϕ-M and ϕ-H, while the leanest case ϕ-L shows smaller temperature amplitudes, in line with having the lowest temperature RMS at the time of ignition, cf. Fig. 1 (bottom right). The particle devolatilization progress in Fig. 2 (illustrated by particle color, see definition in Rieth et al. [4]) shows increasing C_{dev} at the time of ignition with increasing equivalence ratio, as will be discussed in more detail next.

Fig. 3 (top) shows the temperature scatter from all Eulerian cells of the CP-DNS, while Fig. 3 (bottom) solely shows data extracted from cells that contain fuel particles (fp). The full scatter plot of case ϕ-L in Fig. 3 (top left) shows that at the time of (mean) ignition the mixture fraction is distributed around stoichiometry and the highest temperatures are located slightly on the rich side of stoichiometric where two temperature branches can be identified. Considering the reduced gas temperature scatter limited to regions with fuel particles in Fig. 3 (bottom left) it can be observed that the upper temperature branch is located around particles with higher values of C_{dev}, whereas the lower branch is due to areas where particles still feature a lower devolatilization progress. The scatter plots for the stoichiometric case ϕ-M in Fig. 3 (middle) exhibit a wider distribution of mixture fraction values around stoichiometry and a distinct peak near $f \approx 0.09$. The reduced scatter in fuel particle regions shows that the highest temperature occurs around fully devolatilized particles, while regions with low C_{dev} have not ignited yet. Accompanying calculations of strained laminar counterflows featuring volatiles mixing with the oxidizer composition from the CP-DNS (not shown) confirm that the peak temperature under strained conditions is located slightly on the rich side of stoichiometric, in line with the trends in Fig. 3. Fig. 3 (right) shows that the mixture fraction range of case ϕ-H at ignition is narrow and that all fuel particles are completely devolatilized. Comparing with the mixture fraction RMS in Fig. 1 (top right) this can be explained by the fact that the instant of mean ignition of the rich case ϕ-H is considerably later than for cases ϕ-L and ϕ-M, at

a time when the mixture fraction RMS has already reduced considerably from its peak.

With the CP-DNS data for cases ϕ-L, ϕ-M, and ϕ-H now available, the next sections examine the prediction quality of MMC for these cases.

4.2. Conventional MMC with constant parameters

We now explore the predictive capabilities of the conventional MMC approach with the constant conditioning parameters given in Table 3. As already described in Section 3.2, a wide set of MMC-LES model parameter sets to recover the three DNS cases ϕ-L, ϕ-M and ϕ-H was investigated. The major MMC parameters that we varied were the MMC-LES resolution (from fairly standard 1L/1E to very sparse 1L/4E) and the parameters for particle pairing. For the latter, case C-f represents close coupling in reference mixture fraction space, case C-r enforces small physical distances and the intermediate case C-m represents a balanced mix of conditioning in both physical and mixture fraction space, i.e., Eqs. (11) and (12), corresponding to best practice in multiphase MMC.

4.2.1. Conventional MMC predictions of cases ϕ-L and ϕ-M

For both the lean and the stoichiometric DNS cases (i.e., ϕ-L and ϕ-M) the conventional MMC approach with constant conditioning parameters works remarkably well and the CP-DNS data can be fully recovered, see Appendix A. This is particularly true when MMC conditioning is strictly enforced in physical space (green lines in Fig. A.9(a) and (b)), while minor deviations in the predictions of both mixture fraction and temperature RMS are obtained for cases C-f and C-m (red and blue lines in Fig. A.9(a) and (b)). Overall, the MMC predictions are not very sensitive to sparseness, although the 1L/1E results are slightly more accurate than the sparsest 1L/4E case in Fig. A.9(a) and (b). The reason for the effect of the conditioning sets C-f, C-m and C-r will now be explored in more detail for the rich DNS case ϕ-H, where the MMC model parameter variation has the strongest impact.

4.2.2. Conventional MMC predictions of case ϕ-H

The conventional MMC predictions of the DNS case ϕ-H are presented in Fig. 4 which shows the time evolution of the volatile mixture fraction RMS (1st row), mean gas temperature (2nd row), gas temperature RMS (3rd row) and time rate of change of the mean gas temperature (4th row) for the three MMC-LES resolutions 1L/1E to 1L/4E (left to right). Since the present MMC-LES data is evaluated in an a priori manner by post-filtering the DNS, Fig. 4 omits profiles of the mean volatile mixture fraction, where a perfect match of DNS and MMC is achieved. The trends with increasing sparseness from left to right in Fig. 4 for the rich case ϕ-H agree with the ones already observed for the lean and stoichiometric cases ϕ-L and ϕ-M in Fig. A.9(a) and (b). While the sparsest case 1L/4E cannot recover the CP-DNS very well, the results for the typical MMC resolutions 1L/1E and 1L/2E are good if a reasonable set of conventional MMC parameters is used.

Inspecting the effect of conditioning of stochastic particle pairing for mixing in Fig. 4 it can be observed that the best conventional MMC predictions are obtained when conditioning strictly in physical space (C-r, green), followed by conditioning in combined physical and reference mixture fraction space (C-m, blue) and pure conditioning on mixture fraction (C-f, red), with the latter results deviating the most from the DNS data. The temporal profiles of MMC case C-r are in good agreement with the DNS for both mixture fraction and gas temperature RMS, the mean gas temperature, and also the derivative of the latter, such that the ignition delay time of DNS case ϕ-H is recovered well by MMC. We note, however, that this result may not fully generalise. This is because in the present approach the coupling of stochastic particle pairs is inherently coupled with the two-phase coupling of stochastic and fuel particles (via Eq. (15)), where conditioning on f may be favorable for stochastic particles, whereas close coupling in physical space may be more accurate for two-phase coupling. For the present work, we retain the simple and easy-to-implement expression given by Eq. (15).

Table 4
Predicted ignition delay times t_{ign} and relative ignition time errors Δt_{ign} from constant (Section 4.2) and dynamic (Section 4.3) MMC both with 1L/2E compared with the CP-DNS case ϕ-H (DNS reference value in **bold**). For constant MMC, the mixing time scale parameter C_ξ is kept fixed at the standard value 0.1, while for dynamic MMC $\alpha_f = 0.03$ is kept fixed, while the effect of a variation of C_ξ across the range [0.01, 0.5] is explored. A negative/positive sign of Δt_{ign} indicates early/delayed ignition predicted by MMC.

Constant MMC				
Settings	C-f	C-m	C-r	**CP-DNS**
t_{ign} [ms]	1.94	2.23	2.34	**2.31**
Δt_{ign}	−16.02%	−3.46%	+1.30%	–
Dynamic MMC ($\alpha_f = 0.03$)				
C_ξ	0.01	0.06	0.1	0.5
t_{ign} [ms]	2.76	2.31	2.18	1.70
Δt_{ign}	+19.48%	0.0%	−5.63%	−26.41%

Extracting the peak values of the time derivative of the mean gas temperature from Fig. 4 for the intermediate MMC resolution 1L/2E, one obtains mean ignition times t_{ign} predicted by MMC of 1.94 ms, 2.23 ms, and 2.34 ms for cases C-f, C-m, and C-r respectively, while the CP-DNS equivalent is 2.31 ms (cf. vertical green lines in Fig. 1). For ease of comparison, the ignition delay times and their relative errors compared with the DNS case ϕ-H extracted from conventional MMC (this section) are shown in the upper part of Table 4 (with the lower part on *dynamic MMC* discussed in the next section). It can be seen that the MMC predictions of ignition delay time are considerably different for different conditioning strategies, covering a range from −16.02 % to +1.30 %, as explored in more detail for the intermediate MMC resolution 1L/2E next.

Fig. 5 (left) shows scatter plots of gas temperature vs. volatile mixture fraction at the times of ignition extracted from the MMC cases at 1L/2E for C-f (top), C-m (middle), and C-r (bottom). Comparing with Fig. 4 (middle column) it can be observed that MMC case C-f predicts strongly earlier mean ignition, which explains the hot scatter points for MMC (red) in Fig. 5 (top left), while the DNS scatter (black) extracted at the same time $t = 1.94$ ms corresponds to largely unreacted gas. However, MMC cases C-m and C-r in Fig. 5 (left column, middle/bottom) show comparable scatter between DNS and MMC, since the ignition delay times predicted by MMC (2.23 and 2.34 ms) are considerably closer to the DNS value of 2.31 ms.

The differences in the ignition times of the MMC cases C-m and C-r compared to C-f are further explored on the right of Fig. 5. Here, contour plots (grayscale) and selected isolines (yellow, orange, red, and dark-red) of mixture fraction at the same times as on the left are overlaid with stochastic particles shown in green. Stochastic particle pairs formed *within* the shown layer in the x-range $0.45L_x \leq x \leq 0.55L_x$ are indicated as green dots linked by black lines, whereas particles that are paired *outside* the shown layer are illustrated as green crosses. Focusing on case C-f in Fig. 5 (top right), one can observe that particle pairs span across large physical distances of up to half the domain width, as can be expected for strict conditioning in reference mixture fraction space and not in physical space at all. In contrast, case C-r enforces closeness in physical space, Fig. 5 (bottom right). The intermediate case C-m with balanced conditioning in combined mixture fraction and physical space shows increased physical mixing distances, but mostly retains the mixing of nearby stochastic particles, see Fig. 5 (middle right).

Fig. 6 compares probability density distributions of the realized stochastic particle pair distances in mixture fraction space d_f (left column) and physical space d_x (right column) to their nominal counterparts f_m, r_m for the rich DNS case ϕ-H at 1L/2E as a function of time. The mean values of d_f and d_x at every time instant are shown as red dashed lines, while the constant nominal values f_m and r_m are marked as black horizontal lines. The results for case C-f in Fig. 6 (top) show that the mean realized particle pair distances in both mixture fraction and physical space remain lower than their nominal values at all times of the simulation. For case C-r in Fig. 6 (bottom) the nominal

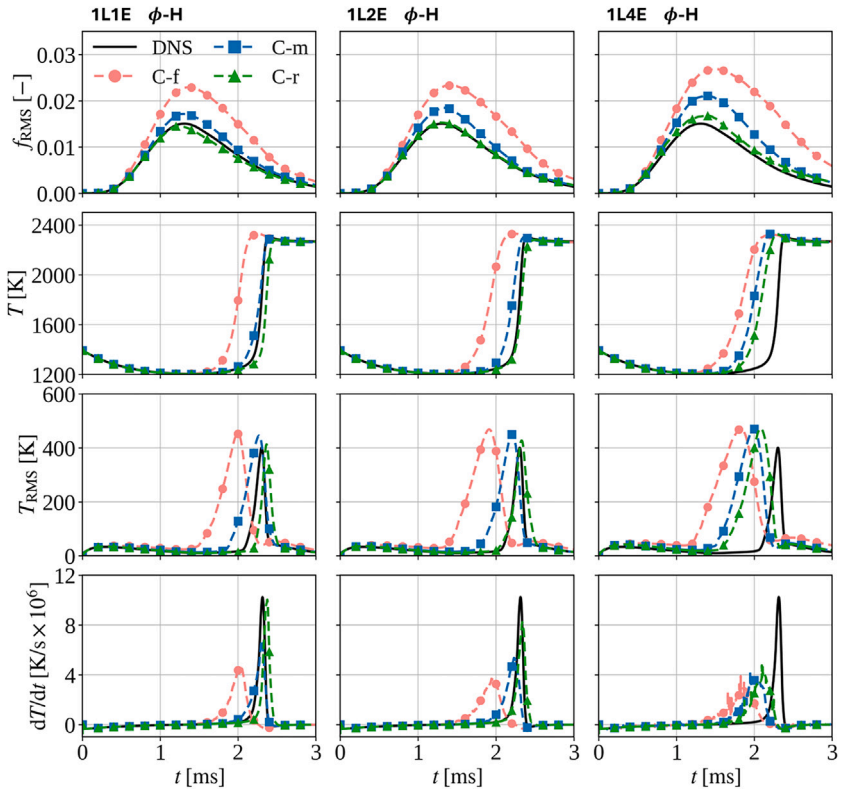

Fig. 4. Comparison of the CP-DNS data with *conventional MMC* for the case ϕ-H. Time evolution of mixture fraction RMS (row 1), mean gas temperature (row 2), gas temperature RMS (row 3) and time rate of change of the mean gas temperature (row 4), for MMC-LES resolutions 1L/1E (left column), 1L/2E (middle column) and 1L/4E (right column). The DNS data is shown in black, whereas parameter sets C-f, C-m and C-r are colored in red, blue and green. (For interpretation of the references to color in this figure legend, the reader is referred to the web version of this article.)

value $f_m = 1.0$ cannot be reached by d_f at any time, while the nominal value $r_m = 0.0076$ mm (1% of the average particle distance Δ_L) is not attained by d_x. Instead, the mean physical distance of particle pairs is around 0.76 mm (i.e., $\approx \Delta_L$ for case 1L/2E) at all times, indicating that for case C-r nearby particles are always selected for mixing, as expected. Finally, case C-m in Fig. 6 (middle) shows that the nominal values f_m and r_m are approximately reached by the mean realized values d_f and d_x at intermediate simulation times, while d_f and d_x remain far below their nominal counterparts at the beginning and near the end of the simulation. The reason for this behavior is attributed to the availability (or lack thereof) of a wide range of volatile mixture fraction values to choose from, which is highest at intermediate simulation times and zero at early and late times, see Fig. 1 (top left).

Overall, we find that -while results in reasonable agreement with the DNS data can be achieved- conventional MMC does not allow for a consistent match of the realized particle pair distances with their nominal counterparts for the present solid fuel ignition and combustion case throughout the entire transient process, even if best-practice multiphase MMC is conducted.

4.3. MMC with dynamic parameter scaling

We now explore the predictive capabilities of the newly proposed *dynamic MMC parameter scaling* approach. As already outlined in Section 2.3, in this approach the MMC conditioning parameters f_m and r_m, as well as their two-phase equivalents f_m^* and r_m^*, are no longer constant but, instead, dynamically scaled with scaling factor α_f according to Eq. (14). While the evaluation of the dynamic MMC approach has been performed for all DNS cases ϕ-L, ϕ-M and ϕ-H, the latter (rich) case showed the strongest sensitivity and we therefore limit our discussion to case ϕ-H.

In analogy to Fig. 6 for *conventional MMC*, Fig. 7 compares probability density distributions of the realized stochastic particle pair distances in mixture fraction space d_f (left column) and physical space d_x (right column) to their nominal counterparts f_m, r_m for the rich DNS case ϕ-H at 1L/2E as a function of time, now using *dynamic MMC*. The scaling factor α_f for dynamic MMC is varied across a wide range 0.01, 0.03 and 0.09, where $\alpha_f = 0.03$ corresponds to the standard value in conventional multiphase MMC.

Inspecting Fig. 7 (left column) it can be observed that the nominal values of f_m (black lines) are dynamically adapted over time for all values of α_f, being zero at early and late times of the simulation and peaking at intermediate times around 1.4 ms. As expected by virtue of Eq. (14) this trend is in line with the temporal profiles of the filtered volatile mixture fraction previously illustrated as the green shaded area in Fig. 1 (top left), where $\tilde{f}_{\max} - \tilde{f}_{\min}$ becomes largest at intermediate times. The red lines corresponding to the mean values of the d_f distribution follow the same trend, indicating that particle pairs in accordance with their nominal conditioning parameters are found throughout the entire simulation. The factor α_f directly scales the overall level of f_m as expected, where the resulting mean values of d_f match f_m well for α_f in the interval [0.01, 0.03], while the mean d_f is overall too low for $\alpha_f = 0.09$.

The profiles of r_m and (mean) d_x in Fig. 7 (right column) are in good agreement, showing that suitable distances between particle pairs in physical space are found. With the value of f_m dynamically obtained, r_m is also updated at every time step according to Eq. (13), where larger values of f_m (due to larger α_f) will result in smaller nominal physical distances r_m and vice versa, as shown in Fig. 7 (right column). Inspecting Eq. (13), at first sight, one would expect an inverse trend between f_m and r_m, such that the profiles of r_m and d_x in the right column of Fig. 7 should have a minimum at intermediate times. However, for the present case, spatial gradients of the mixture fraction are first generated by devolatilization and later destroyed again by (continuously forced) turbulence, as shown by the profiles of the mean gradient of the filtered volatile mixture fraction averaged over the HIT

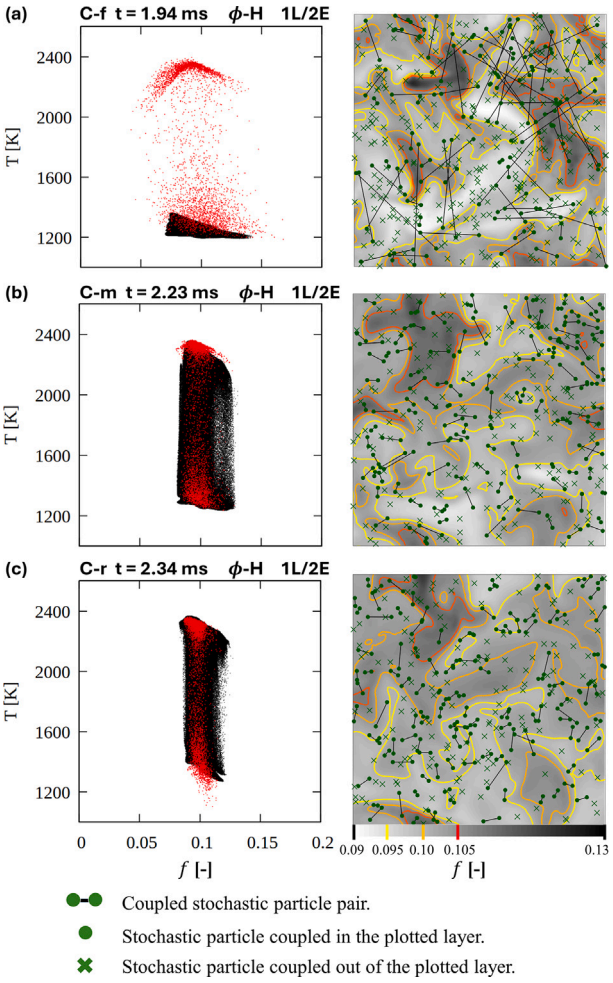

Fig. 5. Left: Scatter plots of gas temperature vs. volatile mixture fraction comparing DNS (black) with *conventional MMC* (red) sets *C-f* (top), *C-m* (middle), and *C-r* (bottom) for the rich DNS case ϕ-H at 1L/2E. The shown times 1.94, 2.23, and 2.34 ms correspond to the ignition delay times t_{ign} extracted from the three MMC cases and the DNS scatter is presented at the same times. Right: Visualization of stochastic particle pairing at the same times; background shows mixture fraction in the y-z plane at $x = 0.5L_x$ with isolines 0.095 (yellow), 0.10 (Orange), and 0.105 (red). Particles are selected in a planar section defined by $0.45L_x \leq x \leq 0.55L_x$; solid green circles mark in-region pairings, whereas green crosses mark pairings outside the shown x-layer. (For interpretation of the references to color in this figure legend, the reader is referred to the web version of this article.)

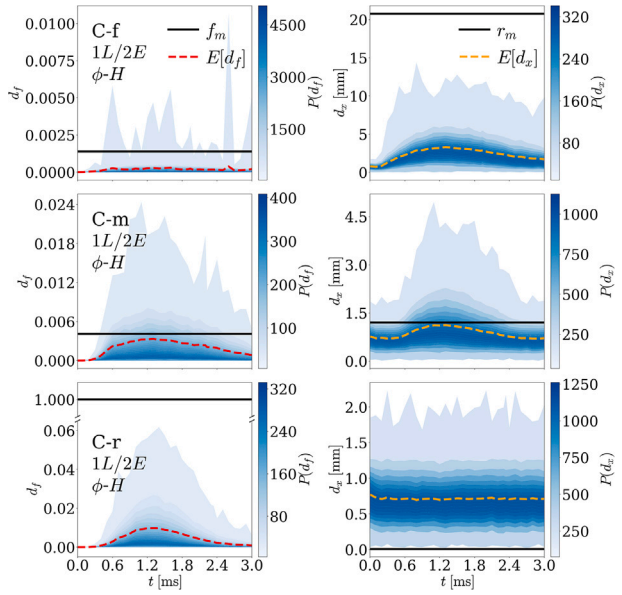

Fig. 6. Probability density distributions of the realized stochastic particle pair distances in mixture fraction space d_f (left column) and physical space d_x (right column) vs. time for case ϕ-H at 1L/2E using *conventional MMC*. The color bar on the right denotes the probability density of the pairing distances d_f and d_x. The mean realized particle distances d_f, d_x are shown as red dashed lines and compared with their nominal counterparts f_m, r_m as black horizontal lines for parameter sets *C-f* (top), *C-m* (middle), and *C-r* (bottom). (For interpretation of the references to color in this figure legend, the reader is referred to the web version of this article.)

domain vs. time. This trend of $d\tilde{f}/dn$ compensates the otherwise inverse trend of $r_m = f(1/f_m)$ in Eq. (13), such that the profiles of r_m and d_x remain approximately constant over time. The two-phase coupling parameters f_m^* and r_m^* are scaled according to Eq. (15). They therefore exhibit the same relative trends as f_m and r_m, and are not shown here for brevity. Overall, we find that with the proposed dynamic MMC approach, a dynamically-adapted set of MMC conditioning parameters can be obtained, which is matched by the realized particle pair distances in both physical and mixture fraction space across the entire simulation time. A scaling factor of $\alpha_f = 0.03$ that corresponds to the previous recommendation by Sontheimer et al. [21] for conventional MMC works well for case ϕ-H shown in Fig. 7, as well as for all other DNS cases considered in the present work, see Appendix B. We therefore retain $\alpha_f = 0.03$ and recommend it as the appropriate scaling factor for the dynamic model, at least in the present HIT context.

Finally, Fig. 8 shows temporal profiles of the mixture fraction RMS, mean gas temperature, gas temperature RMS and time rate of change of the mean gas temperature from dynamic MMC with $\alpha_f = 0.03$ for case

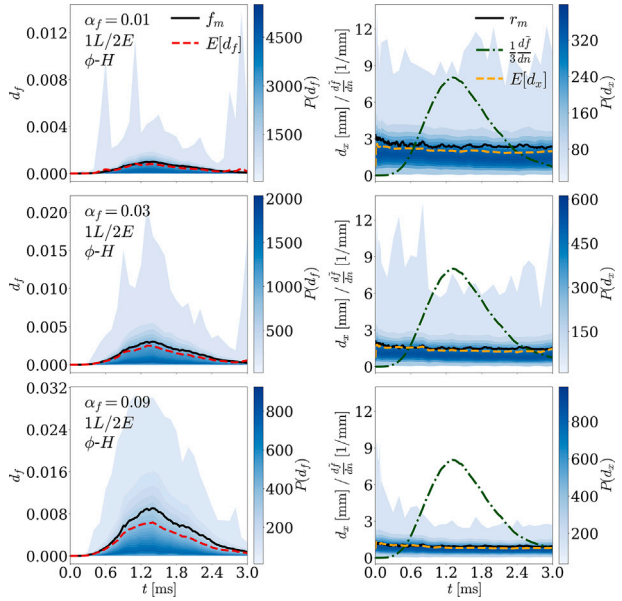

Fig. 7. Probability density distributions of the realized stochastic particle pair distances in mixture fraction space d_f (left column) and physical space d_x (right column) vs. time for case ϕ-H at 1L/2E using *dynamic MMC*. The color bar on the right denotes the probability density of the pairing distances d_f and d_x. The mean realized particle distances d_f, d_x are shown as red dashed lines and compared with their nominal counterparts f_m, r_m as black lines for different values of the dynamic MMC scaling factor α_f of 0.01 (top), 0.03 (middle), and 0.09 (bottom). The green dashed-dotted lines in the right column show the gradients of the filtered volatile mixture fraction spatially-averaged across the HIT domain (scaled by 1/3 for clarity). (For interpretation of the references to color in this figure legend, the reader is referred to the web version of this article.)

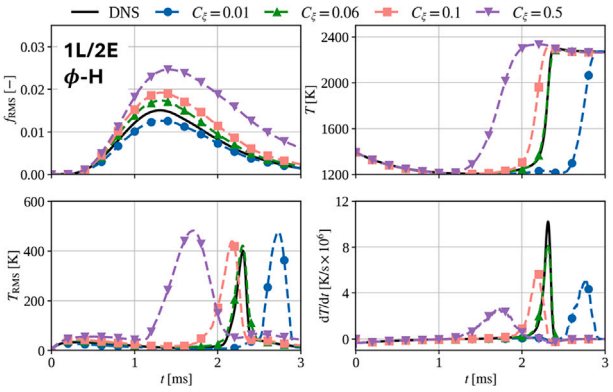

Fig. 8. Comparison of the CP-DNS data with *dynamic MMC* for the rich DNS case ϕ-H. Time evolution of mixture fraction RMS (top left), mean gas temperature (top right), gas temperature RMS (bottom left) and time rate of change of the mean gas temperature (bottom right), for MMC-LES resolution 1L/2E with scaling factor $\alpha_f = 0.03$. The DNS data is shown in black, whereas corresponding MMC data is shown in color for values 0.01, 0.06, 0.1 and 0.5 of the *a-ISO* mixing time scale model parameter C_ξ. (For interpretation of the references to color in this figure legend, the reader is referred to the web version of this article.)

ϕ-H at MMC resolution 1L/2E. Results are shown across the range [0.01, 0.5] of parameter C_ξ in the *a-ISO* mixing time scale model, see Eq. (10). Fig. 8 shows that MMC predictions are a strong function of parameter C_ξ, with very small values (0.01) leading to overly late ignition, whereas very large values (0.5) lead to considerably earlier ignition than in the reference DNS dataset. The standard value for constant C_ξ (0.1) leads to an overall reasonable agreement with the DNS time evolution, albeit somewhat early ignition is predicted. Further tuning of C_ξ to a value of 0.06 leads to almost perfect agreement of the dynamic MMC result with the DNS data. This is also reflected quantitatively in the lower part of Table 4 which compares the ignition delay times predicted by dynamic MMC with $\alpha_f = 0.03$ across the selected range of C_ξ values to the corresponding DNS result. While very small $C_\xi = 0.01$ yields around 20% later ignition compared with the DNS, a very large $C_\xi = 0.5$ predicts the mean ignition event to occur ≈ 26% earlier than in the DNS. With around 5% earlier ignition, the standard value $C_\xi = 0.1$ lies in the same ballpark as conventional MMC with best-practice parameter settings (case *C-m*, ≈ 3.5% earlier ignition), while the zero deviation of ignition delay for $C_\xi = 0.06$ in Table 4 confirms the almost perfect agreement shown in Fig. 8. However, while it has previously been pointed out in [24] that values of $C_\xi < 0.1$ may be more suitable for MMC, it remains an open question if this finding can easily be generalized. Future work will need to establish if the standard value $C_\xi = 0.1$ for the subgrid scalar variance (inherited from LES turbulence modeling for reacting flows [34,35] methods) needs further adjustment for dynamic MMC or not. The trends of the MMC predictions with respect to parameter C_ξ found for case *ϕ-H* in Fig. 8 are also observed for the DNS cases *ϕ-L* and *ϕ-M*, as shown in Appendix C. However, for these cases the dependence on C_ξ is considerably weaker than for case *ϕ-H*.

Overall, we find that the newly-proposed dynamic scaling approach for MMC conditioning leads to realizable particle pair distances in both volatile mixture fraction and physical space (Fig. 7), as well as reasonable MMC predictions of the transient physics of solid particle heat-up, devolatilization, ignition and volatile combustion (Fig. 8). A comparison of the computational cost for the dynamic scaling approach vs. conventional MMC (omitted for brevity) did not show any systematic overhead of dynamic MMC. However, it needs to be noted that the computational cost for MMC is only a fraction of the cost for the DNS in the present a priori approach. As a result, the observed differences were likely due to natural run-to-run variability -dominated by the DNS- on the compute cluster.

5. Conclusions

The present study generated CP-DNS validation data for the heat-up, ignition, and volatile combustion of pulverized coal particles in HIT under a wide range of global equivalence ratios. The resulting database was then used to assess the MMC conditioning strategy a priori by comparing the conventional MMC approach with *constant parameters* for particle pair selection against a newly proposed *dynamic scaling* approach. The main conclusions are as follows:

- Reliable and well-defined validation data for the MMC-LES model development were generated by CP-DNS. The DNS data will be provided to the research community and can be used for future model development. While the present DNS dataset is somewhat limited by the inherent assumptions of HIT, it provides further validation in addition to combustion experiments and their inherent uncertainties.
- The *conventional MMC* approach with *constant parameters* can reproduce DNS if the parameters are appropriately selected. However, this requires prior information on the scalar range and case-dependent calibration. Moreover, the prescribed parameters f_m and r_m are not consistently realized by the selected particle pairs throughout the transient combustion process.
- The proposed *dynamic scaling* approach addresses this inconsistency by updating the conditioning parameters based on the instantaneous range of the filtered volatile mixture fraction. With $\alpha_f = 0.03$, the prescribed values of $f_m(t)$ and $r_m(t)$ remain closely matched by the realized mean particle pair distances $d_f(t)$ and $d_x(t)$ throughout the simulation.
- The MMC predictions still show some sensitivity to the mixing time scale parameter C_ξ in the *a-ISO* model. The standard value $C_\xi = 0.1$ already gives satisfactory predictions, while $C_\xi = 0.06$ provides a closer match to the present DNS data for rich conditions.

Future work will aim to extend the present research towards fully coupled a posteriori MMC-LES, considering spatially inhomogeneous flows governed by shear and dynamic two-phase coupling. A full MMC-LES model for coal combustion will also need to include char conversion.

CRediT authorship contribution statement

Shiqi Meng: Writing – original draft, Visualization, Validation, Software, Methodology, Formal analysis, Data curation. **Tien Duc Luu:** Writing – review & editing, Validation, Software, Methodology. **Ali Shamooni:** Writing – review & editing, Validation, Software, Methodology. **Andreas Kronenburg:** Writing – review & editing, Supervision, Resources, Conceptualization. **Oliver T. Stein:** Writing – review & editing, Supervision, Resources, Project administration, Funding acquisition, Conceptualization.

Declaration of competing interest

The authors declare that they have no known competing financial interests or personal relationships that could have appeared to influence the work reported in this paper.

Acknowledgements

The authors acknowledge the financial support from the Chinese Scholarship Council (grant no. 201906420087, S. Meng) and from the Deutsche Forschungsgemeinschaft, Germany for project number 450158108. We are grateful for HPC time on bwHPC and Horeka.

Appendix A. Results of *conventional MMC* for DNS cases ϕ-L and ϕ-M

Using the constant MMC parameters from Table 3, Fig. A.9(a) and (b) show that the conventional MMC approach recovers the CP-DNS results well for both ϕ-L and ϕ-M. The best agreement is obtained when MMC

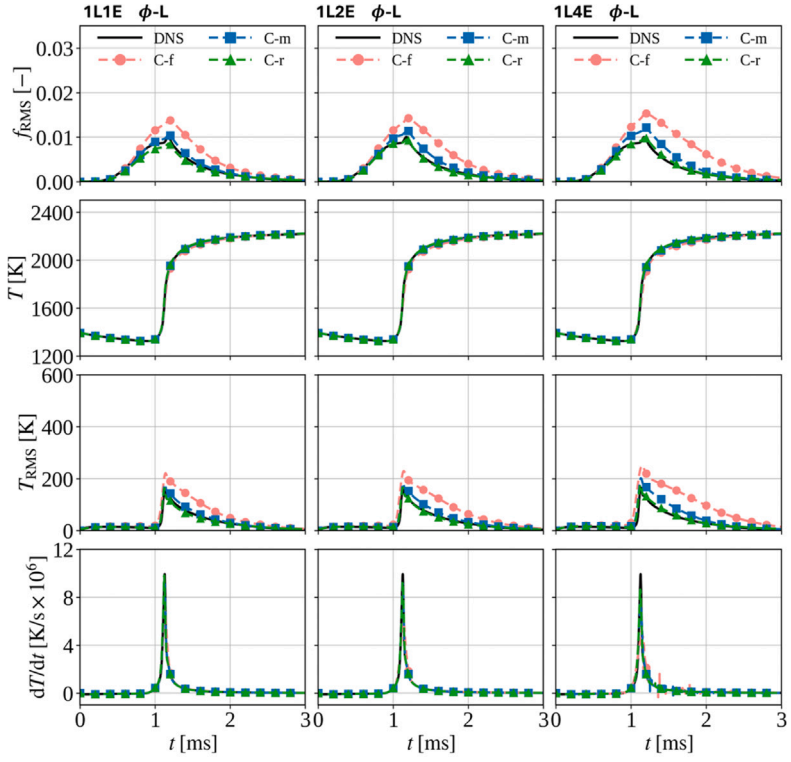

(a) ϕ-L

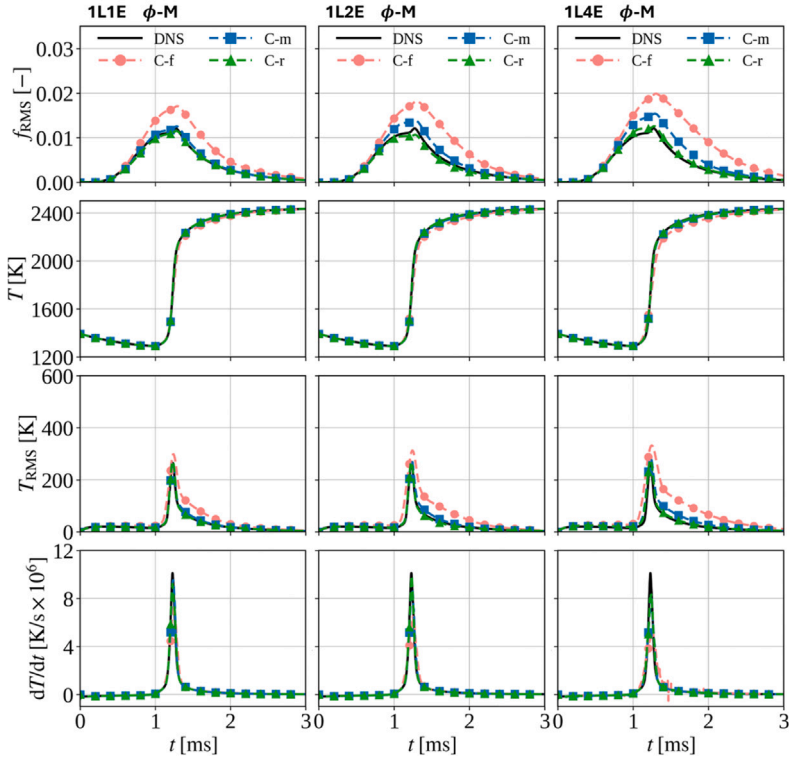

(b) ϕ-M

Fig. A.9. DNS case ϕ-L (a) and ϕ-M (b): Comparison of CP-DNS data with conventional MMC. Shown are mixture fraction RMS (row 1), mean gas temperature (row 2), gas temperature RMS (row 3), and its time derivative (row 4) for MMC-LES resolutions 1L/1E (left column), 1L/2E (middle column), 1L/4E (right column). DNS in black. C-f, C-m, C-r in red, blue, and green. (For interpretation of the references to color in this figure legend, the reader is referred to the web version of this article.)

conditioning is strictly enforced in physical space (case C-r), whereas cases C-f and C-m show only minor RMS deviations.

Appendix B. Results of *dynamic MMC* particle pairing for all DNS cases

Fig. B.10 shows the stochastic particle pairing statistics obtained with the dynamic MMC approach for DNS cases ϕ-L, ϕ-M, and ϕ-H at MMC resolutions 1L/1E, 1L/2E, and 1L/4E. For all DNS cases and MMC resolutions, $\alpha_f = 0.03$ keeps the mean pairing distances $E(d_f)$ and $E(d_x)$ consistent with the dynamically evaluated reference parameters f_m and r_m, respectively.

Appendix C. *a-ISO* mixing time scale model parameter sensitivity study for cases ϕ-L and ϕ-M

Fig. C.11 compares the CP-DNS data with dynamic MMC predictions using the a-ISO model for DNS cases ϕ-L and ϕ-M at the 1L/2E resolution with $\alpha_f = 0.03$. Overall, the results show that both $C_\xi = 0.06$ and 0.1 provide good agreement with the CP-DNS data, while $C_\xi = 0.06$ yields slightly improved performance compared with $C_\xi = 0.1$.

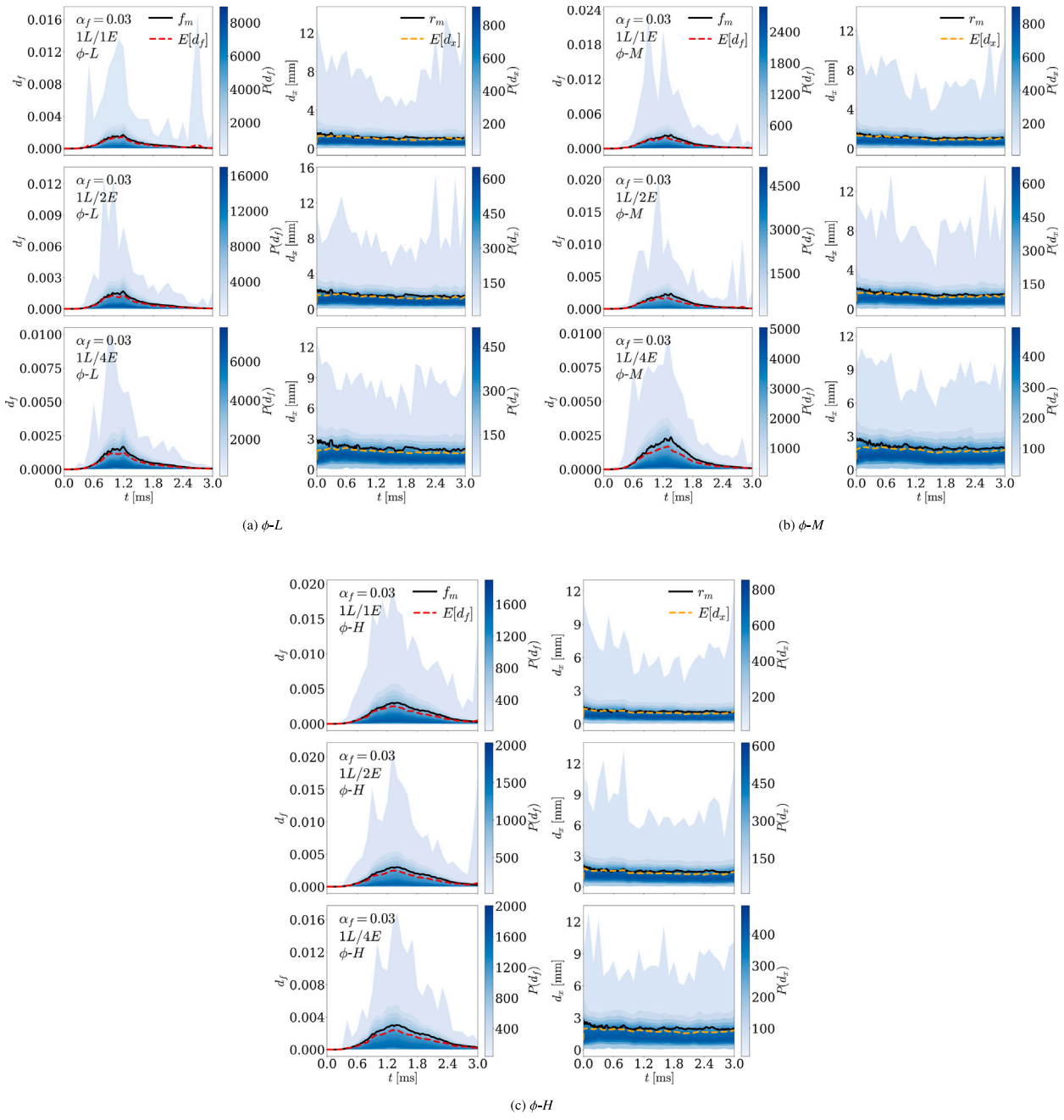

Fig. B.10. Stochastic particle pairing results for DNS cases ϕ-L (a), ϕ-M (b), and ϕ-H (c) at MMC resolutions 1L/1E, 1L/2E, and 1L/4E. Temporal evolution of f_m and r_m (solid black lines) vs. mean values $E(d_f)$ and $E(d_x)$ (dashed red lines). The color bars on the right of each subfigure denote the probability density of the pairing distances d_f and d_x. (For interpretation of the references to color in this figure legend, the reader is referred to the web version of this article.)

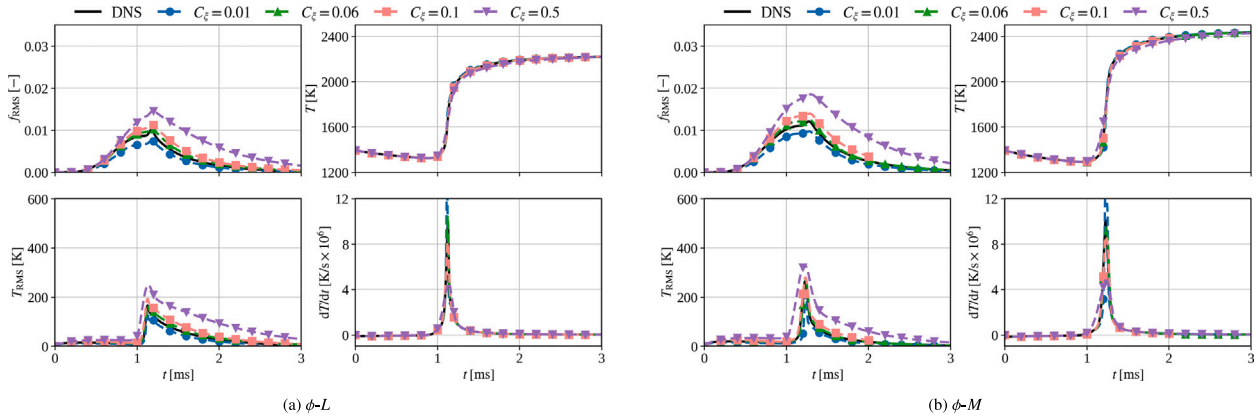

(a) ϕ-L (b) ϕ-M

Fig. C.11. DNS cases ϕ-L and ϕ-M: Comparison of CP-DNS data with dynamic MMC at 1L/2E resolution ($\alpha_f = 0.03$). Each panel shows mixture fraction RMS (top left), mean gas temperature (top right), gas temperature RMS (bottom left), and its time derivative (bottom right). DNS in black. MMC in color for $C_\xi = 0.01, 0.06, 0.1, 0.5$ using the a-ISO model. (For interpretation of the references to color in this figure legend, the reader is referred to the web version of this article.)

Appendix D. Scaling ratio sensitivity test of the two-phase coupling model for case ϕ-H

To examine the sensitivity of the present results to the prescribed ratio $r_m/r_m^* = f_m/f_m^*$, an additional parametric check was conducted for the best-performing configuration identified in the present study, i.e., 1L/2E MMC resolution, $\alpha_f = 0.03$ of the *dynamic scaling factor*, and $C_\xi = 0.06$ of the *a-ISO* mixing time scale model in the case of ϕ-H. The baseline value used in the manuscript is 1.66. Two additional values, 0.83 and 2.49, corresponding to a ±50% variation from the baseline value, were also tested. As shown in Fig. D.12, all the predicted results are very close to each other.

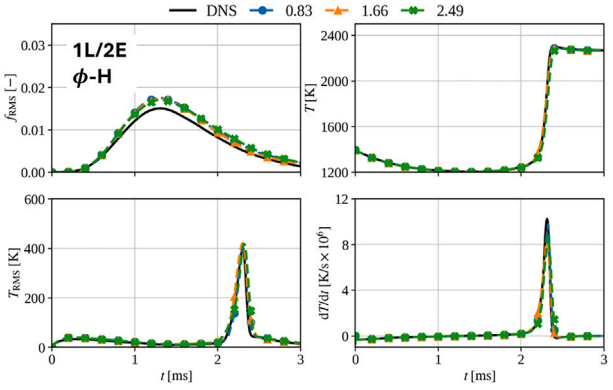

Fig. D.12. Sensitivity of the predicted results to the MMC two-phase coupling ratio $r_m/r_m^* = f_m/f_m^*$. The tested values are 0.83, 1.66, and 2.49, corresponding to a ±50% variation around the baseline value of 1.66. (For interpretation of the references to color in this figure legend, the reader is referred to the web version of this article.)

Data availability

The data will be made available online in the flame database section of the *Clean Solids Conversion (CSC)* workshop series at https://csc.ebi.kit.edu/index.php.

References

[1] Dorokhov V, Kuznetsov G, Nyashina G, Strizhak P. Composition of a gas and ash mixture formed during the pyrolysis and combustion of coal-water slurries containing petrochemicals. Environ Pollut 2021;285:117390.
[2] Prabhakaran SS, Swaminathan G, Joshi V. Combustion and pyrolysis kinetics of Australian lignite coal and validation by artificial neural networks. Energy 2022;242:122949.
[3] Hasse C, Debiagi P, Wen X, Hildebrandt K, Vascellari M, Faravelli T. Advanced modeling approaches for CFD simulations of coal combustion and gasification. Prog Energy Combust Sci 2021;86:100938.
[4] Rieth M, Kempf A, Kronenburg A, Stein OT. Carrier-phase DNS of pulverized coal particle ignition and volatile burning in a turbulent mixing layer. Fuel 2018;212:364–74.
[5] Luu TD, Zhang J, Gärtner J, Meng S, Kronenburg A, Li T, Løvås T, Stein OT. Single particle conversion of woody biomass using fully-resolved and Euler-Lagrange coarse-graining approaches. Fuel 2024;368:131600.
[6] Luu TD, Shamooni A, Kronenburg A, Braig D, Mich J, Nguyen B-D, Scholtissek A, Hasse C, Thäter G, Carbone M, Frohnapfel B, Stein OT. Carrier-phase DNS study of particle size distribution effects on iron particle ignition in a turbulent mixing layer. Proc Combust Inst 2024;40(1–4):105297.
[7] Tufano G, Stein OT, Kronenburg A, Frassoldati A, Faravelli T, Deng L, Kempf A, Vascellari M, Hasse C. Resolved flow simulation of pulverized coal particle devolatilization and ignition in air-and O_2/CO_2-atmospheres. Fuel 2016;186:285–92.
[8] Tufano G, Stein OT, Kronenburg A, Gentile G, Stagni A, Frassoldati A, Faravelli T, Kempf A, Vascellari M, Hasse C. Fully-resolved simulations of coal particle combustion using a detailed multi-step approach for heterogeneous kinetics. Fuel 2019;240:75–83.
[9] Tufano G, Stein OT, Wang B, Kronenburg A, Rieth M, Kempf AM. Coal particle volatile combustion and flame interaction. Part I: Characterization of transient and group effects. Fuel 2018;229:262–9.
[10] Shamooni A, Debiagi P, Wang B, Luu TD, Stein OT, Kronenburg A, Bagheri G, Stagni A, Frassoldati A, Faravelli T, Kempf AM, Wen X, Hasse C. Carrier-phase DNS of detailed NO_x formation in early-stage pulverized coal combustion with fuel-bound nitrogen. Fuel 2021;291:119998.
[11] Poinsot T, Veynante D. Theoretical and numerical combustion. R.T. Edwards; 2005.
[12] Gao F. A large eddy simulation scheme for turbulent reacting flows. Stanford Univ. Annual Research Briefs, 1993; 1993.
[13] Colucci P, Jaberi F, Givi P, Pope SB. Filtered density function for large eddy simulation of turbulent reacting flows. Phys Fluids 1998;10(2):499–515.
[14] Pope SB. PDF methods for turbulent reactive flows. Prog Energy Combust Sci 1985;11(2):119–92.
[15] Klimenko A, Cleary M. Convergence to a model in sparse-Lagrangian FDF simulations. Flow Turbul Combust 2010;85:567–91.
[16] Klimenko A, Pope SB. The modeling of turbulent reactive flows based on multiple mapping conditioning. Phys Fluids 2003;15(7):1907–25.
[17] Cleary M, Klimenko A. A detailed quantitative analysis of sparse-Lagrangian filtered density function simulations in constant and variable density reacting jet flows. Phys Fluids 2011;23(11).
[18] Vo S, Stein OT, Kronenburg A, Cleary M. Assessment of mixing time scales for a sparse particle method. Combust Flame 2017;179:280–99.
[19] Khan N, Cleary M, Stein OT, Kronenburg A. A two-phase MMC-LES model for turbulent spray flames. Combust Flame 2018;193:424–39.
[20] Kirchmann J, Kronenburg A, Stein OT, Cleary M. Two-phase sparse-Lagrangian MMC-LES of dilute ethanol spray flames. Proc Combust Inst 2021;38(2):3343–50.
[21] Sontheimer M, Kronenburg A, Stein OT. Two-phase coupling for MMC-LES of spray combustion. Proc Combust Inst 2021;38(2):3361–9.
[22] Sontheimer M, Kronenburg A, Stein OT. A comparative study of two-phase coupling models for a sparse-Lagrangian particle method. Proc Combust Inst 2023;39(2):2643–52.
[23] Zhao L, Cleary M, Stein OT, Kronenburg A. A two-phase MMC-LES model for pyrolysing solid particles in a turbulent flame. Combust Flame 2019;209:322–36.
[24] Sharma E, De S, Cleary M. A fully dynamic mixing time-scale model for the sparse Lagrangian multiple mapping conditioning approach. Combust Flame 2022;238:111872.

[25] Bassenne M, Urzay J, Park G, Moin P. Constant-energetics physical-space forcing methods for improved convergence to homogeneous-isotropic turbulence with application to particle-laden flows. Phys Fluids 2016;28(3).
[26] Shamooni A, Stein OT, Kronenburg A, Kempf A, Debiagi P, Li T, Dreizler A, Böhm B, Hasse C. Fully-resolved simulations of volatile combustion and NO_x formation from single coal particles in recycled flue gas environments. Proc Combust Inst 2023;39(4):4529–39.
[27] Kobayashi H, Howard J, Sarofim A. Coal devolatilization at high temperatures. In: Symposium (international) on combustion, 16. Elsevier; 1977. p. 411–25.
[28] Luu TD, Shamooni A, Zhou Y, Kronenburg A, Stein OT. Analysis of the overlap of devolatilisation and char conversion during single coal particle burning using a detailed multi-step kinetic approach. Fuel 2026;421:138969.
[29] Curl R. Dispersed phase mixing: I. theory and effects in simple reactors. Aiche J 1963;9(2):175–81.
[30] Sreenivasan K. Fractals and multifractals in fluid turbulence. Annu Rev Fluid Mech 1991;23(1):539–604.
[31] Sontheimer M. Analysis of sparse-Lagrangian two-phase coupling using direct numerical simulation [Ph.D. thesis]. University of Stuttgart; 2024.
[32] Kazakov A, Frenklach M. DRM: detailed and reduced reaction mechanisms for methane combustion. 2025. http://combustion.berkeley.edu/drm/ [Accessed: June 2025].
[33] Galindo-Lopez S, Salehi F, Cleary M, Masri A, Neuber G, Stein OT, Kronenburg A, Varna A, Hawkes E, Sundaram B, Klimenko AY, Ge Y. A stochastic multiple mapping conditioning computational model in OpenFOAM for turbulent combustion. Comput Fluids 2018;172:410–25.
[34] Branley N, Jones W. Large eddy simulation of a turbulent non-premixed flame. Combust Flame 2001;127(1–2):1914–34.
[35] Navarro-Martinez S, Kronenburg A, Mare FD. Conditional moment closure for large eddy simulations. Flow Turbul Combust 2005;75(1):245–74.